JPET Fast Forward. Published on June 12, 2019 as DOI: 10.1124/jpet.119.256693
This article has not been copyedited and formatted. The final version may differ from this version.

Cellular Uptake and Efflux of Palbociclib *In Vitro* in Single Cell and Spheroid Models

M. Jove[1,a], J. A. Spencer[2,b], M. E. Hubbard[3], E. C. Holden[3], R. D. O'Dea[3], B. S. Brook[3], R. M. Phillips[4], S. W. Smye[5], P. M. Loadman[2,c], C. J. Twelves[6]

1. Institut Català d'Oncologia, Medical Oncology Department, Barcelona, Spain.
2. Institute of Cancer Therapeutics, University of Bradford, Bradford BD7 1DP, UK
3. School of Mathematical Sciences, University of Nottingham, University Park, Nottingham NG7 2RD, UK
4. School of Applied Sciences, University of Huddersfield, Queensgate, Huddersfield HD1 3DH, UK
5. School of Medicine, University of Leeds, Leeds LS2 9JT, UK
6. University of Leeds and Leeds Teaching Hospitals NHS Trust, St James's University Hospital, Leeds LS9 7TF, UK

a, b. Joint first authors

a, c. Corresponding authors

Running title: Cellular uptake and efflux of palbociclib

Corresponding authors:

Paul M Loadman

p.m.loadman@bradford.ac.uk

Address: Institute of Cancer Therapeutics, University of Bradford, Bradford, BD7 1DP

Phone: +44 1274 233228

Maria Jove

mjove@iconcologia.net

Address: Institut Català d'Oncologia. Medical Oncology department.

Av. Gran Via de L'Hospitalet 199-203 | 08908 L'Hospitalet de Llobregat |Barcelona

Phone: +34 932607744 | Fax: +34 932607741

Number of text pages: 27

Number of tables: 2

Number of figures: 5

Number of references: 37

Number of words in the abstract: 226

Number of words in the introduction: 750

Number of words in the discussion: 1498

List of non-standard abbreviations:

CDK	cyclin-dependent kinase
BC	breast cancer
SCS	single cells in suspension
PK	pharmacokinetic
5-FU	5-Fluorouracil
Rb	retinoblastoma
pRb	phospho-retinoblastoma
HR	hormone receptor
HER2	human epidermal growth factor receptor 2
EMA	European Medicines Agency
FDA	US Food and Drug Administration
MP	mobile phase
MeCN	acetonitrile
ECACC	European Collection of Authenticated Cell Cultures
mAb	monoclonal antibody
ECL	enhanced chemiluminescence

JPET Fast Forward. Published on June 12, 2019 as DOI: 10.1124/jpet.119.256693
This article has not been copyedited and formatted. The final version may differ from this version.

Abstract

Adequate drug distribution through tumours is essential for treatment to be effective. Palbociclib is a cyclin-dependent kinase (CDK) 4/6 inhibitor approved for use in patients with hormone receptor (HR) positive, HER2 negative metastatic breast cancer (BC). It has unusual physicochemical properties, which may significantly influence its distribution in tumour tissue. We studied the penetration and distribution of palbociclib *in vitro*, including the use of multicellular three-dimensional models and mathematical modelling. MCF-7 and DLD-1 cell lines were grown as single cell suspensions (SCS) and spheroids; palbociclib uptake and efflux were studied using liquid chromatography-tandem mass spectrometry (LC-MS/MS). Intracellular concentrations of palbociclib for MCF-7 SCS (C_{max} 3.22μM) and spheroids (C_{max} 2.91 μM) were 32 and 29 fold higher and in DLD-1, 13 and 7 fold higher, respectively than the media concentration (0.1 μM). Total palbociclib uptake was lower in DLD-1 cells than MCF-7 cells both in SCS and in spheroids. Both uptake and efflux of palbociclib were slower in spheroids than SCS. These data were used to develop a mathematical model of palbociclib transport that quantifies key parameters determining drug penetration and distribution. The model reproduced qualitatively most features of the experimental data and distinguished between SCS and spheroids, providing additional support for hypotheses derived from the experimental data. Mathematical modelling has the potential for translating *in vitro* data into clinically relevant estimates of tumour drug concentrations.

Significance statement

This study explores palbociclib uptake and efflux in single cell suspension and spheroid models of cancer. Large intracellular concentrations of palbociclib are found after drug exposure. The data from this study may aid understanding of the intratumoural pharmacokinetics of palbociclib which is useful in understanding how drug distributes within

JPET Fast Forward. Published on June 12, 2019 as DOI: 10.1124/jpet.119.256693
This article has not been copyedited and formatted. The final version may differ from this version.

tumour tissue and optimising drug efficacy. Bio-mathematical modelling has the potential to derive intratumoural drug concentrations from plasma pharmacokinetics in patients.

Introduction

For cancer therapeutics to be effective, drug concentrations must exceed a threshold level within cancer cells for a period of time sufficient to ensure the desired effect. Pharmacokinetic resistance, the ineffective delivery of the drug to the cell, has been recognised as an important contributor to treatment failure (Minchinton and Tannock, 2006). The tumour microstructure plays an important role in pharmacokinetic resistance, since cancer drugs have to penetrate and distribute throughout the tumour to be optimally effective (Minchinton and Tannock, 2006). The physicochemical properties of each drug also influences its delivery and distribution; the molecular weight, polarity, pKa and extent of protein binding of a drug all affect how it distributes within the tumour (Fuso Nerini et al., 2014).

Most preclinical intratumoural pharmacokinetic (PK) data relate to cytotoxicity testing *in vitro*, using measures such as IC_{50}, and plasma PK *in vivo*; the majority of preclinical drug distribution studies focus on distribution within individual organs rather than tumours. Although there is a trend to investigate drug penetration using *in vitro* tissue models in pre-clinical drug development (Katt et al., 2016), these studies are not usually routinely performed. *In vitro* multicellular models using cancer cells are feasible and potentially useful to answer questions around drug penetration and distribution at a tissue or cellular level (Barrera-Rodríguez and Fuentes, 2015; Evans et al., 2009; Winter et al., 2019). Multicellular models have been used previously to study intratumoural drug penetration (Godugu et al., 2013; Huang and Gao, 2018). Moreover, some of the PK parameters derived from such models can be used to develop biomathematical models that can improve the understanding of key factors which govern intratumoural drug delivery (Evans et al., 2009; Groh et al., 2014). These models are limited by the parameters obtained from experiments but can potentially optimize the drug development process by identifying promising drug combinations and schedules, supplementing *in vivo* studies which are resource intensive and involve ethical issues, so are limited in number (Altrock et al., 2015).

Once a drug enters clinical trials, plasma PK studies are routine, but there are few drugs for which intratumoural drug concentrations and/or distribution have been studied. One exception is the fluoropyrimidine pro-drug capecitabine, where a PK study confirmed preferential conversion to 5-FU in the tumour (Schüller et al., 2000).

Palbociclib (Ibrance®, Pfizer) is an oral cyclin-dependent kinase (CDK) 4/6 inhibitor that blocks phosphorylation of the retinoblastoma (Rb) protein, a tumour suppressor that controls the transition from G1 to S phase of the cell cycle. Palbociclib, and other CDK4/6 inhibitors, are approved in combination with endocrine therapy in patients with hormone receptor (HR) positive, HER2 negative metastatic breast cancer (BC) (EMA, 2016; Pfizer, 2015), in whom the combination approximately doubles progression-free survival (Clark et al., 2016). Palbociclib has unusual physicochemical properties, which are likely to have a significant influence on its penetration and distribution through tissues. Namely, it has a very large volume of distribution of 2583L and a half-life of 26h, indicating extensive drug binding to peripheral tissues (Flaherty et al., 2012; Schwartz et al., 2011). Furthermore, in whole blood palbociclib distributes preferentially into the cellular component over plasma, with a whole blood to plasma concentration ratio of 1.63 (EMA, 2016). Separate studies have reported plasma palbociclib PK (Smith et al., 2011) and intratumoural palbociclib concentrations *in vivo* (Nguyen et al., 2010) but were based on different doses and routes of administration. Reported clinical plasma concentrations for palbociclib range from 0.062μM to 0.278μM (FDA, 2014; Masuda et al., 2018; Tamura et al., 2016; Taylor et al., 2018). Studies have not reported a direct comparison of both intratumoural and plasma palbociclib concentrations, except in the case of glioblastoma where the issue is complicated by the blood brain barrier (Taylor et al., 2018).

Better understanding of intratumoural palbociclib PK may inform the design of new clinical trials. For example, in studies combining cell cycle inhibitors with chemotherapy, cell cycle arrest may reduce the efficacy of chemotherapy leading to antagonistic rather than

JPET Fast Forward. Published on June 12, 2019 as DOI: 10.1124/jpet.119.256693
This article has not been copyedited and formatted. The final version may differ from this version.

synergistic effects (Dean et al., 2012; McClendon et al., 2012); alternative dosing or scheduling may overcome such a limitation.

We have developed a methodology to study drug uptake and efflux in SCS and 3D spheroid models, quantifying drug concentrations using liquid chromatography-tandem mass spectrometry (LC-MS/MS). This allows us to explore the ability of the drug to move through single cells and spheroids. Using these data, we have developed a mathematical model of palbociclib transport through cancer cells that can quantify the role of key parameters which determine drug penetration and distribution within the tumour.

2. Materials and Methods

2.1. LC-MS/MS methodology:

Stock solutions of palbociclib were prepared at 1 mM in DMSO and stored at -20 ºC. Standard solutions for system calibration were made by further dilutions of stock solutions with a mixture of 50 % mobile phase A (MPA) and 50 % mobile phase B (MPB). For each set of experiments run on LC-MS/MS, calibration curves were created between 0.02 and 10 µM.

Samples were separated and analysed on a Waters 2695 HPLC system in combination with a Waters 2996 Diode Array Detector and a Waters Micromass Ultima triple quadrupole MS. Samples were maintained at 4 ºC in the auto-sampler and 10 µL injected for analysis. Sample separation was carried out on a HiChrom RPB column (250 x 2.1 mm id, 5 µm particle size) maintained at 40 ºC. Gradient elution was applied with 10 % acetonitrile (MeCN) and 0.1 % formic acid for MPA, and 50 % MeCN and 0.1 % formic acid for mobile phase B (MPB) with the following gradient: the starting eluent consisted of 70 % MPA and 30 % MPB, the proportion of MPB increasing linearly to 80 % over 5 min and then returning to 30 % over 1 min. The column was re-equilibrated at starting conditions for 4 min. The flow rate was 0.5 ml min^{-1}, and split post-column with 0.3 ml min^{-1} delivered to the MS. Palbociclib was detected by monitoring the mass transition m/z 448.73 > 381.04 with the instrument

operating in positive mode. A cone energy of 20 eV and collision energy of 20 eV was used with argon gas as the collision gas. The UV signal of palbociclib was also monitored at a wavelength of 365 nm.

2.2. Cell culture:

The human breast cancer cell line MCF-7 and the human colorectal cancer cell line DLD-1 were obtained from our laboratory. Cell line provenance was verified by annual STR profiling (European Collection of Authenticated Cell Cultures [ECACC], Public Health England, Porton Down, Salisbury, UK) and bi-monthly mycoplasma testing was regularly undertaken in house using a MycoProbe Mycoplasma Detection Kit (R&D Systems, Inc, Minneapolis, USA). Both cell lines have the capability to form spheroids.

Cells were cultured in Dulbecco's Modified Eagle's Medium (DMEM) high glucose, supplemented with 10 % foetal bovine serum and 5 % L-Glutamine. For MCF-7 cell line, 1 % insulin was also added. Spheroids were created using 96-well plates previously coated with 1 % Agarose. We optimized spheroid formation to achieve a diameter of approximately 400 µm on day 4 (collecting day) by seeding at 3500 cells ml^{-1} for MCF-7 and 6000 cells ml^{-1} for DLD-1. Spheroid diameter was optimized to avoid the formation of a necrotic core and reduce variability in the subsequent assays. Briefly, spheroids were embedded in paraffin, sectioned and stained with haematoxylin-eosin to visualize their structure and confirm the absence of a necrotic core (Supplementary Figure S3). Cells were maintained in 25 ml tissue culture flasks at 37 ºC in humidified incubator with 5 % CO_2.

2.3. Cell viability:

Both MCF-7 and DLD-1 were treated for 480 min with 0.1 µM of palbociclib, under the conditions described below for both uptake and efflux experiments, with viable cells counted using a haemocytometer and trypan blue.

2.4. Western blots:

JPET Fast Forward. Published on June 12, 2019 as DOI: 10.1124/jpet.119.256693
This article has not been copyedited and formatted. The final version may differ from this version.

We performed western blots of retinoblastoma (Rb), phospho-retinoblastoma (pRb; serine 780), CDK4 and CDK6 as a pharmacodynamics measure of whether palbociclib's mechanism of action was preserved in the cell lines.

MCF-7 and DLD-1 cells were grown as described above and, once confluent, harvested for analysis. Cell pellets were lysed for 10 min on ice in buffer containing a protease and phosphatase inhibitor cocktail mix (Abcam), followed by sonication using 3 x 5 second cycles twice at 40 % power. Samples were tested for protein content by Bradford assay and loaded on to 10 % SDS-polyacrylamide gels at 50 μg $well^{-1}$ protein for separation. A protein ladder was also loaded for molecular weight comparison (PageRuler Plus Prestained Protein Ladder, Fermentas Life Sciences). Separated proteins were then transferred onto a nitrocellulose membrane and incubated with blocking buffer appropriate to the 1° antibody (Ab) for 1 h. Membranes were subsequently incubated with the following 1°Abs overnight at 4°C: CDK4 (D9G3E) Rabbit mAb, CDK6 (DCS83) Mouse mAb, Rb (4H1) Mouse mAb, Phospho-Rb (Ser780) (D59B7) Rabbit mAb, Phospho-Rb (Ser795) Ab and Phospho-Rb (Ser807/811) (D20B12) XP Rabbit mAb. β-Actin Ab was used as a control. Following incubation with the appropriate 2°Ab for 1 h at room temperature, the membranes were incubated with SignalFire ECL Reagent (Cell Signaling Technology Inc.) for 1 min and the signal captured on x-ray film. Exposure time varied from 10 s to 3 min, depending on the antibody used.

2.5. In vitro drug uptake and efflux:

The palbociclib concentration used for uptake and efflux experiments was 0.1 μM. This dose was selected based on reported clinical plasma concentrations (FDA, 2014; Masuda et al., 2018; Tamura et al., 2016; Taylor et al., 2018). A concentration at the lower end of the range was chosen to assure cell viability whilst remaining above the biologically effective dose of 0.06 μM (FDA, 2014).

JPET Fast Forward. Published on June 12, 2019 as DOI: 10.1124/jpet.119.256693
This article has not been copyedited and formatted. The final version may differ from this version.

2.5.1. *Drug uptake:*

One million cells in suspension, or 30 spheroids per time point, were maintained at 37 ºC in Eppendorfs and treated with 1ml of 0.1 µM palbociclib in complete media for 0 to 240 min (0, 5, 10, 20, 40, 60, 120 and 240 min) and 0 to 480 min (0, 5, 10, 20, 40, 60, 120, 240, 360 and 480 min), respectively. At each designated time point, cells were centrifuged at 1000 g for 2 min, media discarded and the cell pellet or spheroids washed three times with phosphate-buffered saline (PBS) before re-suspension in 150 µl of acetonitrile and storing on ice. The cell pellet or spheroids were sonicated twice at 40% power for three x 5 second cycles and six x 5 second cycles, respectively using a Sonoplus HD2070 Homogeniser Ultrasonic (Scientific Laboratory Supplies Limited, UK) to disrupt the cell membranes and release intracellular drug. All samples were then centrifuged at 10,000 g for 5 min. Finally the supernatant was transferred to a new Eppendorf and evaporated using a Genevac personal evaporator at 37 ºC, 8 mbar pressure for approximately 120 min and reconstituted in 30 µl of mobile phase (MPA:MPB, 1:1). Appropriate control samples of untreated cells or spheroids and samples containing drug without cells were also included to ensure the validity of the assay. The method is described in Supplementary Figure S1.

2.5.2. *Drug efflux:*

One million cells in suspension or 30 spheroids were treated with 1 ml of 0.1 µM palbociclib in complete media for 1 hour and 2 hours, respectively at 37 ºC. After incubation with drug, samples were centrifuged at 1000 g for 2 min, media containing drug removed and the cell pellet or spheroids washed three times with PBS. 50 µl of fresh drug-free media was then added and samples incubated for 5 to 240 min (5, 10, 20, 40, 60, 120 and 240 min) and 5 to 480 min (5, 10, 20, 40, 60, 120, 240, 360 and 480 min) for cells and spheroids, respectively. At each designated time point, samples were centrifuged for 2 min at 1000 g and the media transferred to a clean Eppendorf. Both media and cell or spheroid pellets were processed for analysis as described above. The method is described in Supplementary Figure S2.

JPET Fast Forward. Published on June 12, 2019 as DOI: 10.1124/jpet.119.256693
This article has not been copyedited and formatted. The final version may differ from this version.

Protein concentration for each experiment was measured using the Bradford assay. Cell and spheroid volumes were derived from their respective diameters assuming both to be spherical. Diameters were measured accurately using a metric rule under the microscope at 20x and validated by Image J software for scientific analysis. For single cell diameters, at least 50 cell diameters were measured in different passages; the mean cell diameter was used to derive the cell volume. For spheroids, the diameter of 15 spheroids was measured in each experiment and the mean diameter used to calculate the spheroid volume. Each experiment was performed in triplicate.

2.6. Data analysis:

SCS and spheroid pellets were diluted at the end of the experiment in 30 µl MPA. To determine the actual concentration of drug in the cell or spheroid pellets the following equation applied (all volumes in µl):

SCS

Dilution factor = [(volume of a single cell x $1x10^6$ cells) + 30 µl] / volume of a single cell x $1x10^6$ cells

Spheroids

Dilution factor = [(volume of a spheroid x 30 spheroids) + 30 µl] / volume of a spheroid x 30 spheroids.

We also expressed drug concentrations relative to the sample protein concentration for each experiment (drug concentration:protein ratio), which is independent of cell or spheroid volume.

Raw LC-MS data were processed in MassLynx V4.1. and graphs plotted in Graph Pad PRISM 6.

JPET Fast Forward. Published on June 12, 2019 as DOI: 10.1124/jpet.119.256693
This article has not been copyedited and formatted. The final version may differ from this version.

2.7. Statistics:

Statistical comparison of PK parameters (e.g. area under the concentration-time curve; total drug uptake/efflux [AUC], maximum concentration [C_{max}], time at which maximum concentration is observed [T_{max}] and rate of uptake/efflux) between cells and spheroids were made using Graph Pad PRISM 6. Both C_{max} and T_{max} were derived from direct observation of GraphPad PK curves. All graphs were represented with mean plus error bars with three independent data points per time point, therefore we consider that representing descriptive data was more appropriate. Experiments were performed in triplicate which precludes the assumption of a normal distribution of the data, the Mann-Whitney U test was, therefore, used for statistical comparisons. We used coefficient of variation (CV) to determine the technical error of drug uptake and efflux experiments. Technical error was tested performing three repeats in SCS at the 60 min drug uptake time point with a CV of 19.4% and in SCS at the 6 hour drug efflux time point with a CV of 32.5%.

2.8. Mathematical modelling:

The mathematical model used to describe the transport of palbociclib in single cells and in spheroids has been described previously (Hubbard et al., 2017). In summary, the interaction of palbociclib with the microenvironment of cells is restricted to drug binding, and described by a three-compartment model, comprising extracellular space (volume V_1, 1ml for uptake experiments, 50µl for efflux experiments) with a uniform concentration C_1 of free drug, and intracellular space (volume V_2, 1.65µl for DLD-1 and 3.28µl for MCF-7) with concentrations C_2 and C_3 corresponding to free and bound drug respectively. The term “bound” refers to all types of binding taking place within the cell, including to protein, lipids and organelles. It is assumed that binding can be described by a simple kinetic model with drug binding reversibly to sites within the cell. The core model equations are given by:

JPET Fast Forward. Published on June 12, 2019 as DOI: 10.1124/jpet.119.256693
This article has not been copyedited and formatted. The final version may differ from this version.

$$V_1 \frac{dC_1}{dt} = a\, k_1\, (C_2 - C_1)\,,$$
$$V_2 \frac{dC_2}{dt} = a\, k_1\, (C_1 - C_2) - V_2\, k_2\, C_2\, (C_0 - C_3) + V_2\, k_{-2}\, C_3\,,$$
$$V_2 \frac{dC_3}{dt} = V_2\, k_2\, C_2\, (C_0 - C_3) - V_2\, k_{-2}\, C_3\,,$$

where *a* is the total cellular surface area (6.75×10^{-4} m^2 for DLD-1, 1.07×10^{-3} m^2 for MCF-7 cells). These equations contain four parameters that are found using a least-squares fit to the experimental data – these are k_1, the rate of transport across the cell membrane, k_2, the binding rate, k_{-2}, the unbinding rate, and C_0, the concentration of binding sites in the cells.

The model adopts a compartmental approach in which it is assumed that there is a rapid equilibration of concentration within the extracellular volume and that, for SCS, the free and bound fractions of drug are evenly distributed within the intracellular compartment. For spheroid modelling we no longer assume that equilibration of drug throughout the spheroid is instantaneous but instead model the spatial variation of drug concentration within the spheroid using diffusive transport. The spheroid model is derived by means of a multiscale homogenisation technique developed previously (Babuška, 1976; Larsen, 1975; Sanchez-Palencia, 1970), and recently applied to relevant biological contexts (Dalwadi, 2018; Shipley and Chapman, 2010). Full details of the analysis (Supplementary material, Annex 2) is described by Holden, 2018 (Holden, 2018). In brief, this allows for the derivation of a macroscale description of the drug dynamics, based on the kinetic model, which accommodates microscale features of drug transport and binding kinetics.

The spheroid model introduces an additional parameter that represents a diffusion rate, the value of which is found with the other four parameter values using a least-squares fit to the spheroid data (Supplementary material, Annex 1). The numerical model divides the spheroid into a series of concentric layers and it is assumed that the dynamics of drug transport can be attributed to the exchange of free drug between these layers in the spheroids and between the extra- and intra-cellular compartments, and binding/unbinding within the

JPET Fast Forward. Published on June 12, 2019 as DOI: 10.1124/jpet.119.256693
This article has not been copyedited and formatted. The final version may differ from this version.

intracellular compartment. In line with the experimental procedure described above, the parameter-fitting procedure is undertaken for modelling the uptake of drug by initially drug-free cells, and for modelling the efflux of drug from cells initially bathed in drug. The model parameters are estimated for each cell line by fitting to all six available datasets at once (intracellular uptake and intra- and extracellular efflux for both single cells and spheroids).

2.9. Materials:

Palbociclib (PD 0332991), agarose, phosphate-buffered saline, cell culture reagents, DMSO and HPLC grade acetonitrile, water, and formic acid, were all purchased from Sigma-Aldrich, UK. For western blotting all antibodies were purchased from Cell Signalling Technology Inc; all other reagents were purchased from Sigma-Aldrich, UK unless otherwise specified.

3. Results

3.1. *Cell viability assay and western blot:*

Cytotoxic activity for palbociclib has not previously been reported *in vitro*; to ensure cell death did not influence uptake and efflux values obtained in our experiments, the cells were first tested for viability. MCF-7 and DLD-1 cell lines were treated at 0.1 μM of palbociclib for 480 min under the same conditions as those to be used for the uptake and efflux experiments; 98% and 97% of cells were viable for MCF-7 and DLD-1, respectively following incubation with drug.

To account for potential variability between cell lines in uptake/efflux due to binding to the drug target, we tested expression of CDK4 and downstream signalling proteins in the cell lines by performing western blots of retinoblastoma (Rb), phospho-retinoblastoma (pRb) (serine 780), CDK4 and CDK6. Both cell lines were positive for Rb (110kDa), pRb (110kDa) and CDK4 (30kDa) and negative (i.e. below detectable levels) for CDK6 (37kDa). The MCF-7 cell line had higher CDK4 expression than the DLD-1 cell line (Figure 1). A positive blot for

CDK6 in HCC38, a breast cancer cell line, is shown in the Supplementary Figure S4 as a positive control.

3.2. *Uptake:*

Uptake of palbociclib into SCS and spheroids over time was measured in MCF-7 and DLD-1 cell lines (Figure 2A & B, Table 1). In the SCS, the initial rate of change of intracellular concentration was 631.1 and 187.3 nM min^{-1} for MCF-7 and DLD-1, respectively. In contrast, in spheroids the initial rate of uptake (log phase) was 31.2 and 15.6 nM min^{-1} for the MCF-7 and DLD-1 lines, respectively. In SCS the C_{max} of intracellular palbociclib was reached at 10 min then plateaued, whereas in spheroids uptake did not achieve steady state until 120 min in DLD-1 and 240 min in MCF-7, respectively. The intracellular palbociclib C_{max} was far higher than the concentration in the external media, in both cells and spheroids. In MCF-7 the mean C_{max} was 3.22 μM in SCS and 2.91 μM in spheroids; this was 32 and 29 fold higher, respectively, than the treatment concentration of 0.1 μM. In the DLD-1 cell line the mean C_{max} in SCS was 1.28 μM, and 0.68 μM in spheroids; this is almost 13 and 7 fold higher, respectively, than the external media concentration. The difference, in C_{max} between SCS and spheroids was not, however, statistically significant (Mann-Whitney test p=0.36 for MCF-7 line and p=0.2 for DLD-1 line). Moreover, C_{max} was higher in the MCF-7 line than in DLD-1 in both SCS and spheroids; the difference was statistically significant only in SCS (Mann-Whitney test: p= 0.035 for SCS and 0.1 for spheroids).

Total palbociclib uptake, expressed as AUC taken from the drug uptake curve, was lower in DLD-1 (mean $AUC_{(0\text{-}4h)}$ 169 μM.h and 119 μM.h for SCS and spheroids, respectively) than in MCF-7 experiments (mean $AUC_{(0\text{-}4h)}$ 509 μM.h and 368 μM.h for SCS and spheroids, respectively); this difference reached statistical significance in SCS but not the spheroids (Mann-Whitney test: p=0.035 and 0.1, respectively). These results did not differ significantly when expressed as drug:protein ratio, with a similar pattern of drug uptake reaching C_{max} at

10 min in SCS for both cell lines, and at 120 min for DLD-1 and 240 min for MCF-7 spheroids (Supplementary Figure S5).

The initial rate of uptake (log phase) was 10.29 and 2.25 pmol mg^{-1} min^{-1} for the MCF-7 and DLD-1 SCS, respectively. In spheroids the initial rate of uptake (log phase) was 0.29 and 0.10 pmol mg^{-1} min^{-1} for the MCF-7 and DLD-1 lines, respectively. Mean C_{max} in MCF-7 was 53.5 pmol mg^{-1} for SCS and 31.6 pmol mg^{-1} for spheroids. DLD-1 mean C_{max} was 15.29 pmol mg^{-1} and 8.11 pmol mg^{-1}, for cells and spheroids respectively. Total palbociclib uptake, expressed as mean $AUC_{(0\text{-}4h)}$, for the uptake curve in DLD-1 was 2440 h.pmol mg^{-1} and 1510 h.pmol mg^{-1} for SCS and spheroids, respectively, and for MCF-7 was 7535 h.pmol mg^{-1} and 4689 h.pmol mg^{-1} for SCS and spheroids, respectively. The differences in palbociclib uptake of SCS between DLD-1 and MCF-7 for C_{max} and AUC did not reach statistical significance when expressed as drug:protein ratio (p=0.057 and p=0.057, respectively).

3.3. *Efflux:*

Efflux of palbociclib from cells and spheroids was measured over time after one and two hours respectively of drug exposure in MCF-7 and DLD-1 cell lines (Figure 3, Table 2). Drug exposure time prior to efflux experiments was selected based on the time taken to reach C_{max} in uptake experiments. Exposure time was, therefore, longer in spheroids as drug uptake was slower. This ensured the initial intracellular drug concentration was close to steady state before efflux commenced and limited the potential for experimental error.

The rate of change of intracellular concentration of palbociclib during efflux studies in SCS and spheroids was -2.3 and -2.1 nM min^{-1}, respectively in the MCF-7 cell line. In the DLD-1 cell line palbociclib efflux was -0.08 and -0.1 nM min^{-1}, respectively in SCS and spheroids. In MCF-7, efflux equilibrium was achieved somewhat later than in the DLD-1. In SCS efflux equilibrium was reached at 480 min in MCF-7 and 240 min in DLD-1. In spheroid efflux, DLD-1 reached equilibrium at 240 to 360 min, whilst MCF-7 had not yet reached equilibrium by 480 min (the latest time point measured). Again, these results were similar when

JPET Fast Forward. Published on June 12, 2019 as DOI: 10.1124/jpet.119.256693
This article has not been copyedited and formatted. The final version may differ from this version.

expressed as drug to protein ratio (Supplementary Figure S6). The ratio of intracellular to extracellular drug was calculated at each time point (Supplementary Figure S7). In MCF-7 the percentage of intracellular palbociclib remaining at 480 min was 45.14% and 70.76% in the SCS and spheroids, respectively. In DLD-1 the percentage remaining drug was 30.99% and 40.67% in SCS and spheroids, respectively.

3.4. *Mathematical model:*

The results obtained using the mathematical model, shown in Figures 4 and 5, reproduce qualitatively most of the features in the experimental data and distinguish between SCS and spheroid data. The simplicity of the model precludes it from being able to reproduce the decrease in intracellular drug concentrations from their high early values in the SCS uptake experiments as seen in Figures 4 and 5. In particular, the high intracellular drug concentrations visible in the first 30-60 minutes of the SCS uptake experiments are not approximated well by the simulations; by contrast, the model recapitulates the observed concentration time variation for the spheroids reasonably well. The results for DLD-1 do show a very rapid initial increase in intracellular concentrations, but it is much smaller in magnitude than seen in the experiments. For DLD-1, the simulations slightly overestimated the SCS extracellular efflux concentrations and underestimate the spheroid extracellular efflux concentrations, but otherwise fit well to the experimental data. For MCF-7, the fits also qualitatively match the experimental data, though the intracellular concentrations obtained from the simulations slightly overestimate the uptake data and underestimate the efflux data.

Note that the data have been fitted with both a standard least squares fit (shown in Figures 4 and 5) and a χ^2 fit (Supplementary material, Annex 1). There were no significant qualitative differences between the two sets of results. The discrepancies between the observed data and model fits for the SCS data are informative; it is clear that the initial very rapid uptake of drug in the SCS is not described accurately by simple first-order kinetic processes which are

assumed in the model and that an active transport mechanism is more likely, with higher-order terms playing a leading role. Conversely, the agreement between the model and experiment seen in the spheroids, arguably of more relevance in tumours *in-vivo*, confirms that the dominant drug transport processes in the spheroid can be reasonably approximated by first order kinetic/diffusive transport mechanisms.

4.0. Discussion

We developed a methodology to study drug uptake and efflux *in vitro* in 2D and 3D models. For palbociclib we observed very high intracellular drug concentrations compared to the external media drug treatment concentration, with especially rapid uptake in SCS. The mathematical model we developed was able to reproduce most of the features of the experimental data.

Palbociclib uptake experiments showed an initial rapid uptake rate in SCS, with slower uptake in spheroids occurring over 2 hours. In contrast, palbociclib efflux was much slower. Notably, intracellular C_{max} in both SCS and spheroids was up to 32 times higher than the external media concentration. There are a number of potential hypotheses to explain this unusual pattern of drug uptake and efflux, such as active uptake or facilitated transport of the drug across the cell membrane, and very high non-target specific intracellular protein binding. Indeed, palbociclib has high peripheral tissue and protein binding, evidenced by its very large volume of distribution (EMA, 2016). When palbociclib crosses the cell membrane it quickly binds intracellular components leaving a low concentration of free, unbound drug. Drug will, therefore, continue to move into the cell until equilibrium is reached between the free intracellular drug concentration and the media, leading to accumulation inside the cells. In spheroids uptake is much slower as it is likely that intracellular binding saturation must be reached across several layers of cells. The less pronounced differences in efflux between

single cells and spheroids, when compared to uptake, could be explained by a slow intracellular unbinding rate.

There are differences between the data obtained for MCF-7 and DLD-1; the uptake of palbociclib is more prominent in MCF-7, reaching a C_{max} three times higher than in DLD-1. Potential differentials in transporter protein expression between the cell lines are the most likely explanation for this observation; indeed, the presence of an efflux transporter may explain why efflux equilibrium is reached more rapidly in DLD-1 cells. Palbociclib is a known substrate of the efflux transporter Pgp and breast cancer resistance protein (De Gooijer et al., 2015; Parrish et al., 2015); we have not yet explored the different transporters expressed in these two cell lines but this would benefit from further study.

The experimental data are largely supported by the mathematical modelling. Specifically, the parameter values obtained and the model simulations suggest that binding is more rapid than unbinding. As in the experiments, the intracellular concentrations of bound drug at steady state in the uptake model simulations are much higher than the initial concentration of drug in the extracellular media (27 times higher for MCF-7, 6 times higher for DLD-1). These high concentrations are reached quite rapidly; hence, the binding in our model must be rapid, as higher intracellular concentrations than those in the external media could not be achieved by passive transport across the cell membrane alone and there is no facilitated membrane transport in our simple mathematical model. Moreover, the nature of the efflux data requires at least one process to act over a period of hours; only slow unbinding can give the slow decrease in intracellular efflux concentrations because the initial rapid rise in the extracellular concentrations suggests that membrane transport is rapid. This is more pronounced in the simulations of the DLD-1 data, despite the MCF-7 data signifying much faster membrane transport (according to the fitted values of k_1). The slowest process (i.e. unbinding) is faster for MCF-7; therefore, the single-cell simulations settle more rapidly to an equilibrium state, most noticeably in the efflux experiments. However, the ratio of binding to unbinding rates is significantly higher for DLD-1 and consequently the equilibrium is closer to

saturation in the uptake experiments with C_3, the bound drug concentration, reaching approximately 0.6% of C_0 at steady state for MCF-7 compared to approximately 85% for DLD-1.

The model for the spheroid data allows for spatial variation of drug concentrations within each spheroid. For the DLD-1 extracellular efflux data, a rapid initial increase suggests that transport within the spheroid is rapid, allowing unbound drug to escape quickly. This is followed by a slower process in which the bound drug starts to leave the spheroid. A consequence of this rapid intra-spheroid transport is that the model simulations suggest that the SCS and spheroid drug concentrations should both move towards equilibrium at a similar rate when considering uptake. In contrast, the MCF-7 data suggest much slower transport within the spheroid, so both uptake and efflux occur more slowly in spheroids than in SCS. This may, in part, be due to the binding of drug in the periphery of the spheroids delaying the transport of drug to their centres. In the simulations, this difference is a consequence of a much lower diffusion rate (Supplementary material, Annex 1, Table 1) computed when the model parameters are fitted to the MCF-7 data. When a χ^2 fit is used, slower uptake and efflux is again seen in spheroids for MCF-7, but with this parameterisation it is a higher binding rate that induces this behaviour in combination with relatively slow diffusion. This provides some support to the hypothesis that high protein binding might explain the differences between the single cell and spheroid data, though the model also suggests that slow diffusive transport of the drug within the spheroid would affect the concentration profiles in a similar way.

It is difficult to compare our results with the clinical PK parameters of palbociclib as intratumoural concentrations of palbociclib have not been reported in this setting. Moreover, our exposure concentration of 0.1μM should be seen as an artificial representation of steady state extracellular palbociclib concentrations based on reported clinical plasma C_{max} values. Nevertheless, intratumoural palbociclib concentrations from *in vivo* experiments with breast cancer xenografts have been reported. There was, however, no correlation of plasma and

JPET Fast Forward. Published on June 12, 2019 as DOI: 10.1124/jpet.119.256693
This article has not been copyedited and formatted. The final version may differ from this version.

tumour concentrations as the mice bearing breast cancer xenografts for each measurement were treated with different palbociclib doses. In preclinical studies palbociclib intratumoural concentrations have been reported to be 25,163ng/gr (56.2μM) at 6 h after an oral dose of 100mg/kg, and plasma C_{max} of 48ng/ml (0.11μM) after a dose of 2mg/kg (Nguyen et al., 2010; Smith et al., 2011). Human plasma C_{max} from a palbociclib phase I study was 97.4ng/ml (0.21μM) in a multiple dose schedule, but again tumour palbociclib levels were not measured (Flaherty et al., 2012). The high volume of distribution in clinical data supports, however, the high intracellular binding of palbociclib.

Similar experiments have been undertaken with 5-fluorouracil (5FU), a drug with contrasting physicochemical properties to palbociclib, being highly polar with low protein and tissue binding. Images of radiolabelled 5FU showed very rapid uptake in spheroids within a few minutes (Nederman and Carlsson, 1984). Our 5FU uptake and efflux experiments (data not shown) are consistent with this previous publication, showing no difference between SCS and spheroids with similar intracellular and extracellular concentrations at C_{max} and steady state (Jove et al., 2017). In contrast, studies undertaken with doxorubicin, a drug with physicochemical properties more similar to palbociclib, also showed quicker drug uptake in monolayers than in spheroids (Shan et al., 2018; Sutherland et al., 1979).

Our results demonstrate the importance of a drug's physicochemical properties in penetration and distribution within cancer cells. The results obtained using the mathematical model provide additional support for the hypotheses derived from the experimental data regarding the mechanisms that govern the dynamics of palbociclib intratumoural PK. It should be noted that *in vitro* models do not incorporate other factors typically affecting drug delivery *in vivo,* such as tumour stroma or vasculature and our mathematical model omits the effects of active transport, blood supply and interstitial fluid pressure. The

parameterisation itself determines how features in the experimental data are interpreted by the model.

Arguably, the most striking data from this study relate to the large intracellular concentrations that accumulate rapidly after drug exposure. As drugs are assessed *in vitro* for their cytotoxicity or inhibitory effect, as expressed by an IC_{50}, the implications of the intracellular concentrating effect we have seen could be important, with potential consequences for the translation of IC_{50} values into clinical efficacy. If intracellular concentrations *in vitro* are significantly higher than treatment concentration, actual IC_{50} values for some drugs may be much higher than previously thought. This may potentially lead to treatment failures due to sub-optimal dosing. We anticipate that, although some improvements are warranted as more data becomes available, the mathematical model developed here may be used to gain insights into the mechanisms underpinning the data and to obtain accurate predictions of the movement of drugs through tissue based on plasma concentrations. It is also anticipated that this will assist extrapolation from plasma PK data to tumour concentrations, estimating tumour PK data without the need for repeat tumour biopsy.

In conclusion, these are the first *in vitro* models of drug uptake and efflux for palbociclib and together with the mathematical model they are useful to understand palbociclib intratumoural distribution. They could potentially be applied to other drugs to elucidate their intratumoural PK, facilitating improvements in drug delivery and ultimately treatment efficacy.

Acknowledgements:

Special acknowledgment to Spanish Medical Oncology Society (SEOM) for contribution with a personal grant for research abroad of Dr. Jove and Dr. Ramon Salazar for his contribution in this paper.

Author contributions:

Participated in research design: Jove, Spencer, Loadman and Twelves

Conducted experiments: Jove and Spencer.

Contributed analytical tools and performed data analysis: Hubbard, Holden, O'Dea, Brook and Smye.

Wrote or contributed to the writing of the manuscript: Jove, Spencer, Hubbard, Holden, O'Dea, Brook, Phillips, Smye, Loadman and Twelves

References:

Altrock PM, Liu LL and Michor F (2015) The mathematics of cancer: integrating quantitative models. *Nature Reviews Cancer* **15**:730.

Babuška I (1976) Homogenization Approach In Engineering, pp 137-153, Springer Berlin Heidelberg, Berlin, Heidelberg.

Barrera-Rodríguez R and Fuentes JM (2015) Multidrug resistance characterization in multicellular tumour spheroids from two human lung cancer cell lines. *Cancer Cell International* **15**:47.

Clark AS, Karasic TB, DeMichele A, Vaughn DJ, O'Hara M, Perini R, Zhang P, Lal P, Feldman M, Gallagher M and O'Dwyer P (2016) Palbociclib (pd0332991)—a selective and potent cyclin-dependent kinase inhibitor: A review of pharmacodynamics and clinical development. *JAMA Oncology* **2**:253-260.

Dalwadi W, King, Minton (2018) Upscaling diffusion through first-order volumetric sinks: a homogenization of bacterial nutrient uptake. *SIAM Journal on Applied Mathematics* **78**:1300-1329.

De Gooijer MC, Zhang P, Thota N, Mayayo-Peralta I, Buil LCM, Beijnen JH and van Tellingen O (2015) P-glycoprotein and breast cancer resistance protein restrict the brain penetration of the CDK4/6 inhibitor palbociclib. *Investigational New Drugs* **33**:1012-1019.

Dean JL, McClendon AK and Knudsen ES (2012) Modification of the DNA Damage Response by Therapeutic CDK4/6 Inhibition. *The Journal of Biological Chemistry* **287**:29075-29087.

EMA (2016) EPAR summary for the public. EMA/626565/2016, EMEA/H/C/003853: Ibrance, palbociclib, (Agency EM ed), EMA, www.ema.europa.eu.

Evans CJ, Phillips RM, Jones PF, Loadman PM, Sleeman BD, Twelves CJ and Smye SW (2009) A mathematical model of doxorubicin penetration through multicellular layers. *Journal of Theoretical Biology* **257**:598-608.

FDA (2014) NDA 20,7103 Review – Palbociclib (RESEARCH CFDEA ed), FDA, https://www.accessdata.fda.gov/.

Flaherty KT, LoRusso PM, DeMichele A, Abramson VG, Courtney R, Randolph SS, Shaik MN, Wilner KD, O'Dwyer PJ and Schwartz GK (2012) Phase I, Dose-Escalation Trial of the Oral Cyclin-Dependent Kinase 4/6 Inhibitor PD 0332991, Administered Using a 21-Day Schedule in Patients with Advanced Cancer. *Clinical Cancer Research* **18**:568-576.

Fuso Nerini I, Morosi L, Zucchetti M, Ballerini A, Giavazzi R and D'Incalci M (2014) Intratumor Heterogeneity and Its Impact on Drug Distribution and Sensitivity. *Clinical Pharmacology & Therapeutics* **96**:224-238.

Godugu C, Patel AR, Desai U, Andey T, Sams A and Singh M (2013) AlgiMatrix™ Based 3D Cell Culture System as an In-Vitro Tumor Model for Anticancer Studies. *PLoS ONE* **8**:e53708.

Groh CM, Hubbard ME, Jones PF, Loadman PM, Periasamy N, Sleeman BD, Smye SW, Twelves CJ and Phillips RM (2014) Mathematical and computational models of drug transport in tumours. *Journal of the Royal Society Interface* **11**:20131173.

Holden E (2018) New effective descriptions of deformable, adaptively remodelling biological tissue., in *The Centre for Mathematical Medicine and Biology*, University of Nottingham.

Huang B-W and Gao J-Q (2018) Application of 3D cultured multicellular spheroid tumor models in tumor-targeted drug delivery system research. *Journal of Controlled Release* **270**:246-259.

Hubbard ME, Jove M, Loadman PM, Phillips RM, Twelves CJ and Smye SW (2017) Drug delivery in a tumour cord model: a computational simulation. *Royal Society Open Science* **4**:170014.

Jove M, Loadman P, Spencer J, Sulayman L, Wicks J, Race A and Twelves C (2017) Intracellular pharmacokinetics of 5FU and palbociclib: Uptake and efflux in disaggregated cells and 3D models, in *American Association for Cancer Research Annual Conference*, Washington, USA.

Katt ME, Placone AL, Wong AD, Xu ZS and Searson PC (2016) In Vitro Tumor Models: Advantages, Disadvantages, Variables, and Selecting the Right Platform. *Frontiers in bioengineering and biotechnology* **4**:12-12.

Larsen EW (1975) Neutron transport and diffusion in inhomogeneous media. I. *Journal of Mathematical Physics* **16**:1421-1427.

Masuda N, Nishimura R, Takahashi M, Inoue K, Ohno S, Iwata H, Mori Y, Hashigaki S, Muramatsu Y, Nagasawa T, Umeyama Y and Toi M (2018) Palbociclib in combination with letrozole as first-line treatment for advanced breast cancer: A Japanese phase II study. *Cancer science* **109**:803-813.

McClendon AK, Dean JL, Rivadeneira DB, Yu JE, Reed CA, Gao E, Farber JL, Force T, Koch WJ and Knudsen ES (2012) CDK4/6 inhibition antagonizes the cytotoxic response to anthracycline therapy. *Cell Cycle* **11**:2747-2755.

Minchinton AI and Tannock IF (2006) Drug penetration in solid tumours. *Nature Reviews Cancer* **6**:583.

Nederman T and Carlsson J (1984) Penetration and binding of vinblastine and 5-fluorouracil in cellular spheroids. *Cancer Chemother Pharmacol* **13**:131-135.

Nguyen L, Zhong W-Z, Painter CL, Zhang C, Rahavendran SV and Shen Z (2010) Quantitative analysis of PD 0332991 in xenograft mouse tumor tissue by a 96-well

supported liquid extraction format and liquid chromatography/mass spectrometry. *Journal of Pharmaceutical and Biomedical Analysis* **53**:228-234.

Parrish KE, Pokorny J, Mittapalli RK, Bakken K, Sarkaria JN and Elmquist WF (2015) Efflux Transporters at the Blood-Brain Barrier Limit Delivery and Efficacy of Cyclin-Dependent Kinase 4/6 Inhibitor Palbociclib (PD-0332991) in an Orthotopic Brain Tumor Model. *The Journal of Pharmacology and Experimental Therapeutics* **355**:264-271.

Pfizer (2015) FULL PRESCRIBING INFORMATION. IBRANCE® (palbociclib), (Labs P ed), U.S. Food and Drug Administration.

Sanchez-Palencia E (1970) Solutions periodique par rapport aux variables d'espace et applications. *C R Acad Sc Paris* **271**:1129-1132.

Schüller J, Cassidy J, Dumont E, Roos B, Durston S, Banken L, Utoh M, Mori K, Weidekamm E and Reigner B (2000) Preferential activation of capecitabine in tumor following oral administration to colorectal cancer patients. *Cancer Chemotherapy and Pharmacology* **45**:291-297.

Schwartz GK, LoRusso PM, Dickson MA, Randolph SS, Shaik MN, Wilner KD, Courtney R and O'Dwyer PJ (2011) Phase I study of PD 0332991, a cyclin-dependent kinase inhibitor, administered in 3-week cycles (Schedule 2/1). *British Journal of Cancer* **104**:1862-1868.

Shan F, Close DA, Camarco DP and Johnston PA (2018) High-Content Screening Comparison of Cancer Drug Accumulation and Distribution in Two-Dimensional and Three-Dimensional Culture Models of Head and Neck Cancer. *ASSAY and Drug Development Technologies* **16**:27-50.

Shipley RJ and Chapman SJ (2010) Multiscale Modelling of Fluid and Drug Transport in Vascular Tumours. *Bulletin of Mathematical Biology* **72**:1464-1491.

Smith D, Tella M, Rahavendran SV and Shen Z (2011) Quantitative analysis of PD 0332991 in mouse plasma using automated micro-sample processing and microbore liquid

chromatography coupled with tandem mass spectrometry. *Journal of Chromatography B* **879**:2860-2865.

Sutherland RM, Eddy HA, Bareham B, Reich K and Vanantwerp D (1979) Resistance to adriamycin in multicellular spheroids. *International Journal of Radiation Oncology*Biology*Physics* **5**:1225-1230.

Tamura K, Mukai H, Naito Y, Yonemori K, Kodaira M, Tanabe Y, Yamamoto N, Osera S, Sasaki M, Mori Y, Hashigaki S, Nagasawa T, Umeyama Y and Yoshino T (2016) Phase I study of palbociclib, a cyclin-dependent kinase 4/6 inhibitor, in Japanese patients. *Cancer science* **107**:755-763.

Taylor JW, Parikh M, Phillips JJ, James CD, Molinaro AM, Butowski NA, Clarke JL, Oberheim-Bush NA, Chang SM, Berger MS and Prados M (2018) Phase-2 trial of palbociclib in adult patients with recurrent RB1-positive glioblastoma. *Journal of Neuro-Oncology* **140**:477-483.

Winter U, Aschero R, Fuentes F, Buontempo F, Zugbi S, Sgroi M, Sampor C, Abramson DH, Carcaboso AM and Schaiquevich P (2019) Tridimensional Retinoblastoma Cultures as Vitreous Seeds Models for Live-Cell Imaging of Chemotherapy Penetration. *International journal of molecular sciences* **20**:1077.

Footnote:

Funding for this research was provided from a Grant for Translational Research and a grant from Leeds NHS Charitable Trustees.

Legends for Figures:

Figure 1. A representative western blot of CDK4 (30kDa), Rb (110kDa) and pRb phosphorylated at Serine 780 (110kDa) expression in MCF-7 and DLD-1 cell lines. Negative CDK6 (37kDa) not shown.

Figure 2. Palbociclib uptake over time in SCS (A) and spheroids (B) for MCF-7 and DLD-1 cell lines when exposed to media containing 0.1μM palbociclib for up to 480 min. Error bars represent range (n = 3). Difference in MCF-7 and DLD-1 C_{max} for SCS and spheroids, Man Whitney Test p=0.035 and 0.1 respectively.

Table 1. Summary of uptake data for MCF-7 and DLD-1 in SCS and spheroids. Values in brackets represent respective confidence intervals of 95 % (IC95%). Difference in SCS and spheroid C_{max} not significant (MCF-7 p=0.36, DLD-1 p=0.2). Difference in MCF-7 and DLD-1 C_{max} SCS p=0.035 (significant), spheroids p=0.1 (not significant). Difference in DLD-1 and MCF-7 AUC_{SCS} p=0.035 (significant), $AUC_{spheroids}$ p=0.1 (not significant).

Table 2. Summary of efflux data for MCF-7 and DLD-1 in SCS and spheroids. Values in brackets represent respective confidence intervals of 95 % (IC95%).

Figure 3. Palbociclib efflux over time in SCS (A and B) and spheroids (C and D) for MCF-7 and DLD-1 cell lines after a 1 hour (SCS) or 2 hour (spheroids) exposure to media containing 0.1μM palbociclib prior to incubation in drug-free media. Data points represent intracellular concentration of palbociclib remaining at each time point (IN) and effluxed palbociclib measured in the media (OUT). Error bars represent range (n = 3).

Figure 4. Least squares 5-parameter fitting model to all cell and spheroids data for MCF-7. The graphs represent uptake intracellular concentration for SCS (A) and spheroids (D), efflux intracellular concentration for SCS (B) and spheroids (F) and efflux extracellular concentration measured in the media for SCS (C) and spheroids (D). Data points are experimental data as shown in Figures 2 and 3. The line on each plot represents the mathematical simulation.

Figure 5. Least squares 5-parameter fitting model to all cell and spheroids data for DLD-1. The graphs represent uptake intracellular concentration for SCS (A) and spheroids (D),

efflux intracellular concentration for SCS (B) and spheroids (F) and efflux extracellular concentration measured in the media for SCS (C) and spheroids (D). Data points are experimental data as shown in Figures 2 and 3. The line on each plot represents the mathematical simulation.

JPET Fast Forward. Published on June 12, 2019 as DOI: 10.1124/jpet.119.256693
This article has not been copyedited and formatted. The final version may differ from this version.

Table 1.

Uptake	**uptake nM/min**	***Tmax* min**	***C max* µM**	***C max* pmol/mg**	**AUC µM.h**
MCF-7 SCS	631.1	10	3.22µM (2.50-3.93)	53.5 (43.5-63.5)	509 (237.7-779.8)
DLD-1 SCS	187.3	10	1.28 (0.38-2.19)	15.29 (7.92-22.6)	169 (29.73-308.3)
MCF-7 spheroids	31.2	240	2.91 (2.08-3.73)	31.6 (21.8-41.4)	624 (428.1-819.3)
DLD-1 spheroids	15.6	120	0.68 (0.14-1.22)	8.11 (2.30-13.9)	153 (66.29-324.3)

JPET Fast Forward. Published on June 12, 2019 as DOI: 10.1124/jpet.119.256693
This article has not been copyedited and formatted. The final version may differ from this version.

Table 2.

Efflux	**Efflux**	**Time to efflux re-equilibration**	**the percentage of intracellular palbociclib remaining at 480min**
	(nM/min)	**(min)**	**(%)**
MCF-7 cells	2.3	480	45.1 (26.1-64.2)
DLD1 cells	0.08	240	31 (0-68.54)
MCF-7 spheroids	2.1	>480	70.76 (65.65-75.87)
DLD1 spheroids	0.1	240 to 360	40.67 (31.11-50.27)

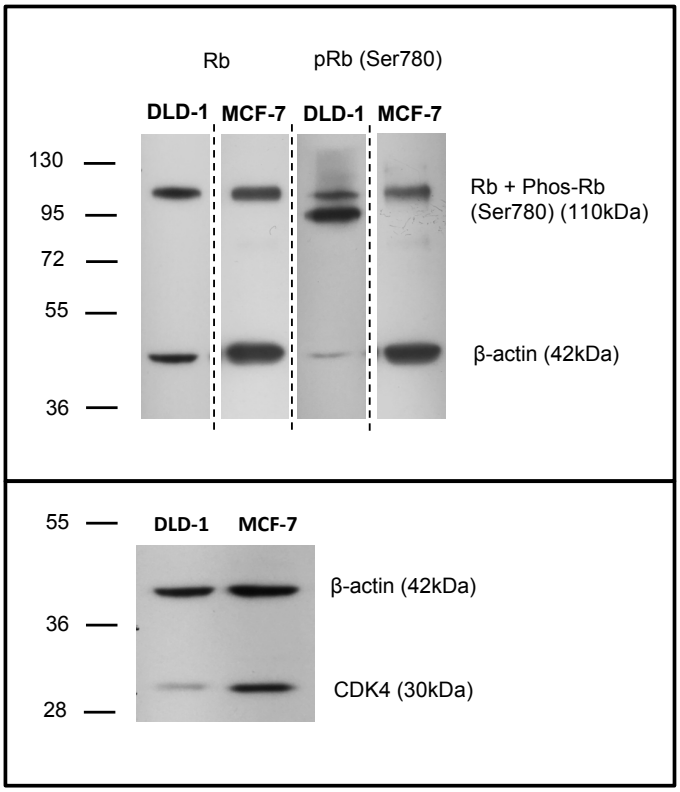

Figure 1. A representative western blot of CDK4 (30kDa), Rb (110kDa) and pRb phosphorylated at Serine 780 (110kDa) expression in MCF-7 and DLD-1 cell lines. Negative CDK6 (37kDa) not shown.

JPET Fast Forward. Published on June 12, 2019 as DOI: 10.1124/jpet.119.256693
This article has not been copyedited and formatted. The final version may differ from this version.

Figure 2.

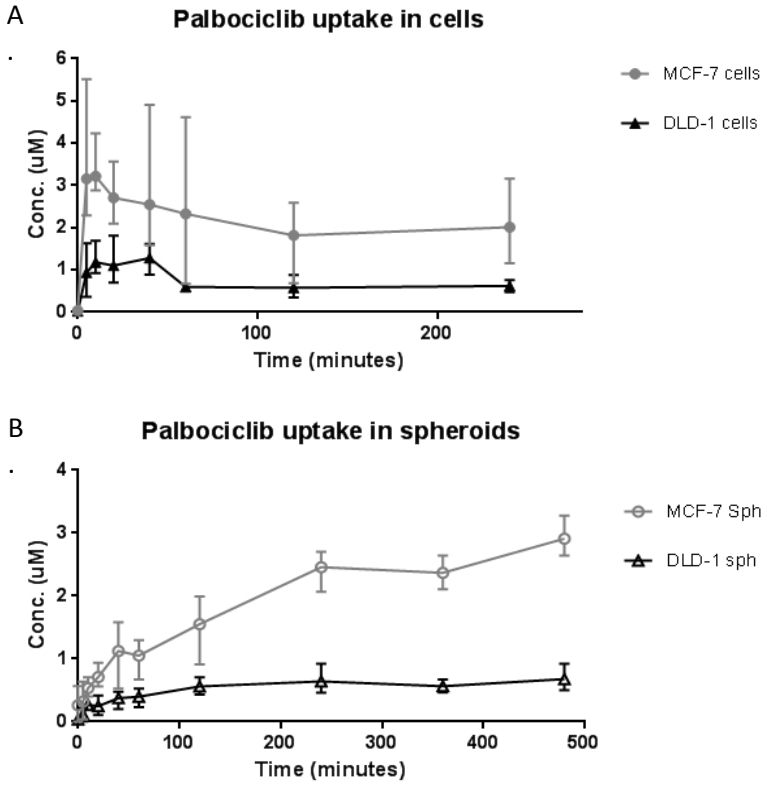

JPET Fast Forward. Published on June 12, 2019 as DOI: 10.1124/jpet.119.256693
This article has not been copyedited and formatted. The final version may differ from this version.

Figure 3.

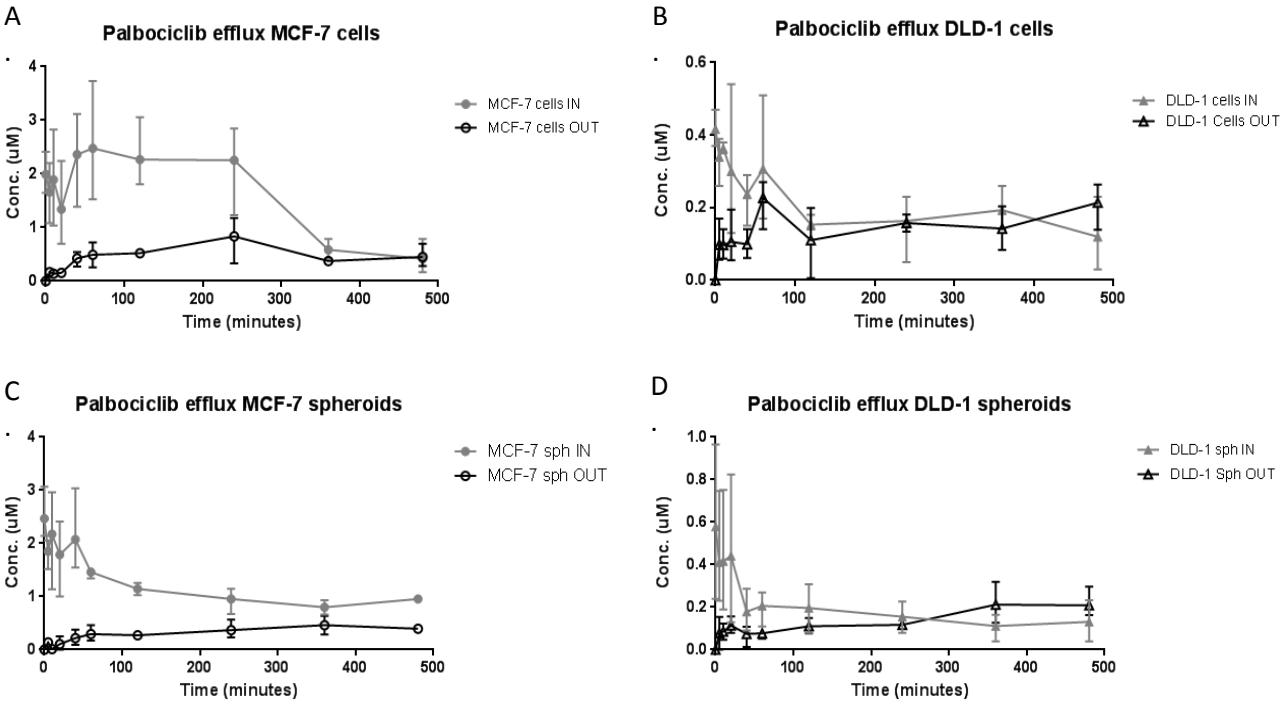

JPET Fast Forward. Published on June 12, 2019 as DOI: 10.1124/jpet.119.256693
This article has not been copyedited and formatted. The final version may differ from this version.

Figure 4.

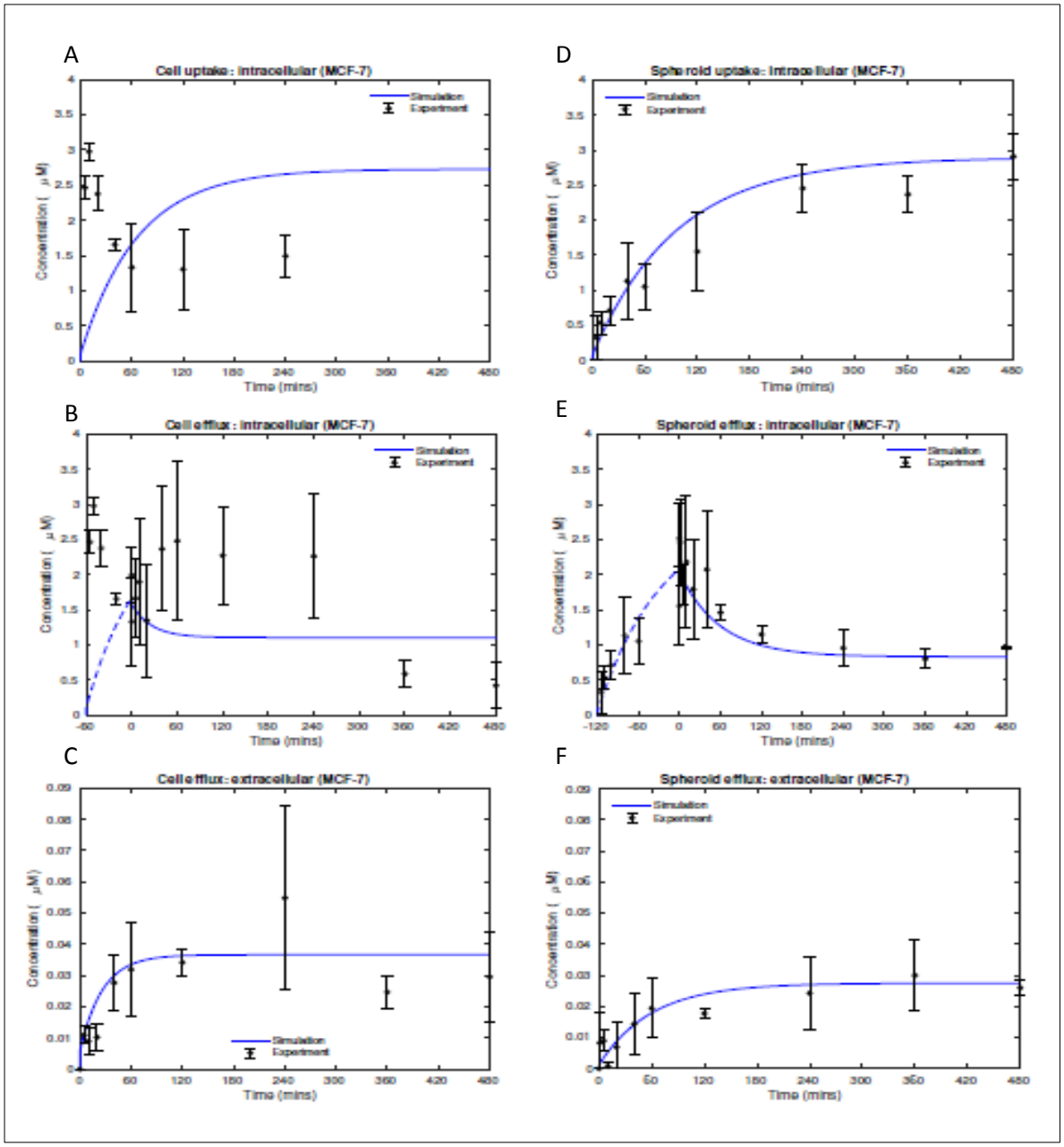

JPET Fast Forward. Published on June 12, 2019 as DOI: 10.1124/jpet.119.256693
This article has not been copyedited and formatted. The final version may differ from this version.

Figure 5.